JOURNAL OF MATERIALS SCIENCE 28 (1993) 6683–6690

The effect of particulate loading on the mechanical behaviour of Al_2O_3/Al Metal-Matrix composites

M. K. AGHAJANIAN, R. A. LANGENSIEPEN, M. A. ROCAZELLA, J. T. LEIGHTON, C. A. ANDERSSON
Applied Composite Technology Unit, Lanxide Corporation, 1300 Marrows Road, PO Box 6077 Newark, DE 19714, USA

An investigation was made to determine the effect of particulate loading on the elastic, tensile, compressive and fracture properties of Al_2O_3/Al metal-matrix composites fabricated by a pressureless-liquid-metal-infiltration process. The elastic modulus was found to be strongly affected by the reinforcement content, falling within the Hashin–Shtrikman bounds. The Young's modulus of the most highly loaded composite was 170 GPa; compare with 65 GPa for the unreinforced alloy. The strength systematically increased with loading, and the rate of increase also increased with loading. The measured yield strengths were nominally the same in both tension and compression; however, the composites possessed far greater ultimate strengths and strains-to-failure in compression than in tension. At 52 vol % reinforcement, yield strengths in tension and compression of 491 and 440 MPa, respectively, were measured, whereas the associated ultimate strengths were 531 and 1035 MPa, respectively. In tension, the yield and ultimate strengths of the base alloy were found to be 170 and 268 MPa, respectively. The composites displayed a nearly constant fracture toughness for all particulate loadings, with values approaching 20 MPa $m^{1/2}$ compared to a value of 29 MPa $m^{1/2}$ for the base alloy. Using fractography, the tensile-failure mechanism was characterized as transgranular fracture of the Al_2O_3 particles followed by ductile rupture of the Al-alloy matrix, with no debonding at the matrix/reinforcement interfaces.

1. Introduction

Discontinuously reinforced metal-matrix composites are of interest for various structural applications due to their improved mechanical properties relative to unreinforced alloys, and their low cost relative to continuous-fibre-reinforced materials. Moreover, these materials are versatile and can be tailored for specific uses by altering the processing of the raw materials. For instance, factors such as the alloy chemistry, the reinforcement shape (particulate, platelet, whisker, etc.), the reinforcement chemistry (Al_2O_3, SiC, etc.), the reinforcement loading, the processing method, post heat treatment, and cold work can have a significant impact on the structural behaviour of the resultant composite. This tailorability, however, presents a challenge to the material developer. The most efficient use of these materials by designers will be limited by their ability to identify the best combination of material characteristics for a given application. Without data which details the independent effects of all the associated variables, this is impossible. To this end, the present paper examines the effect of a single variable, namely the reinforcement loading, on the tensile and compressive properties of metal-matrix composites.

Few sets of systematic data exist within the literature describing the effects of reinforcement loading on the mechanical behaviour of discontinuously reinforced metal-matrix composites. McDanels [1] examined the effect of reinforcement loading in both the SiC-particulate and SiC-whisker-reinforced-Al-alloy-composite systems. The composites were fabricated with a powder metallurgy technique and contained reinforcement loadings from 15 to 40 vol % for the particulate reinforcement and 10 to 30 vol % for the whisker reinforcement. A general increase in both yield and ultimate tensile strength was observed as the loading increased, with the increase in strength attributed to the smaller interparticle spacing in the more highly loaded composites. With the tighter spacing, it was suggested that significant dislocation/reinforcement interactions occurred, resulting in higher strain-hardening coefficients. However, increases in strength with increases in loading were only obtained as long as the composite remained ductile. As the SiC contents reached 30 to 40 vol %, the composites displayed little ductility and the strength increase slowed. Also, working with SiC-reinforced Al composites made by the powder metallurgy method, Papazian and Alder [2] found the tensile yield and ultimate

0022–2461

strengths to be consistently higher with 20 rather than with 8 vol % reinforcement, regardless of the reinforcement type (whisker or particulate), alloy chemistry, or heat-treatment conditions.

McCoy *et al.* [3] produced TiB_2-platelet-reinforced-Al-alloy composites with TiB_2 contents in the range 10 to 25 vol % via a compocasting technique (mechanically mixing the TiB_2 and molten Al alloy, followed by traditional casting into a die). An increase in tensile yield strength was observed as the TiB_2 content was increased from 10 to 18 vol %, but the strength dropped off thereafter with a further increase in particulate loading. These results, however, are complicated by the presence of porosity, which increased as the loading increased. Similarly, Ghosh and Ray [4] fabricated Al_2O_3-particulate-reinforced-Al-alloy composites via compocasting, and investigated reinforcement contents from 0 to 18 vol %. A decrease in ultimate tensile strength with increasing Al_2O_3 content was observed, but as in the work of McCoy *et al.* [3], the results were highly skewed by porosity, which again varied with reinforcement content.

In this study, Al_2O_3-particulate-reinforced-Al-alloy composites were produced by the pressureless infiltration of molten Al alloys into compacts of reinforcing material [5, 6]. (The Process technology is patented by the Lanxide Corporation and named the PRIMEX pressureless-metal-infiltration process.) This technique allows the fabrication of composites with different reinforcement contents, while not affecting the other characteristics of the material. The effect of loading from 25 to 56 vol % is presented, and comparisons are drawn with the unreinforced matrix alloy.

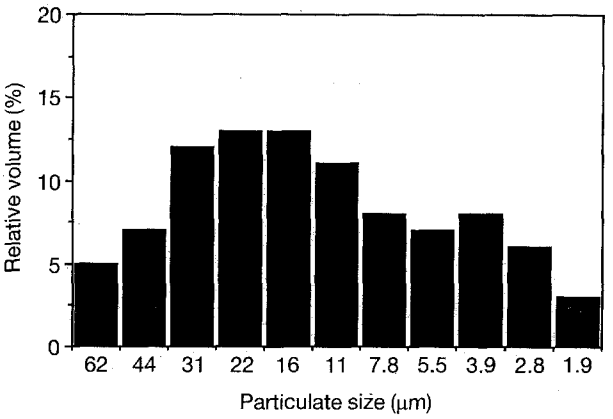

Figure 1 Particle-size distribution of Al_2O_3 reinforcement (measured with a Microtrac model 12-7995 particle-size analyser).

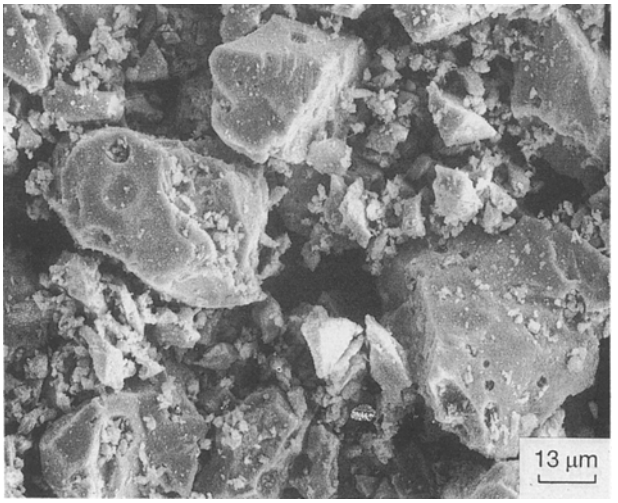

Figure 2 SEM micrograph of Al_2O_3 reinforcement. Note the presence of both coarse particles and fine debris.

2. Materials

2.1. Reinforcement material

All of the composites were produced with the same Al_2O_3 particulate filler. It is a commercially available, sintered and crushed, 99.7% pure, Al_2O_3 powder made up of crystallites with a tabular shape (Alcoa minus 325 mesh T-64 tabular alumina). It is a low-cost powder sold in bulk, typically for refractory applications. The major impurity is 0.16 wt % Na_2O.

This reinforcement material has a wide particle-size distribution, varying from less than 2 μm to greater than 60 μm in diameter, as is shown in Fig. 1. A scanning electron micrograph of the particulate (Fig. 2) shows the existence of both relatively coarse particles and fine debris. The filler particles contain about 3 to 7 vol % closed porosity. Some of these pores, which are spherical in shape, are visible on the surfaces of the larger particles in Fig. 2. The powder was used in the as-received state.

2.2. Composites

The composites were produced by a pressureless-molten-metal-infiltration technique. The requirements for the infiltration have been previously discussed [5, 6], and include the use of a Mg-containing Al alloy and a nitrogenous atmosphere. The present composites were produced by the infiltration of alloy Al–10Mg into Al_2O_3-containing filler beds in nominally pure nitrogen.

The only processing variable investigated was the Al_2O_3 content of the filler bed. The highest particulate loadings (46 vol % and above) were achieved by infiltrating beds of the Al_2O_3 filler packed to different green densities. Composites with lower loadings were fabricated by diluting the Al_2O_3 filler with matrix-metal powder prior to the infiltration step. No settling of the Al_2O_3 during infiltration was observed.

Composites containing 25, 36, 46 and 52 vol % reinforcement were fabricated and characterized. In addition, a composite containing 56 vol % reinforcement was produced and characterized for elastic and compressive properties. (All filler loadings were determined by quantitative image analysis using a Lemont Scientific OASYS System.) Infiltration was carried out in graphite boats at 775 °C. After infiltration the samples were furnace cooled to 675 °C, then the graphite boats were removed from the furnace, placed on a water-cooled chill plate, and covered with high-temperature insulation. This controlled solidification process yielded composites free of solidification porosity. In addition to the composites, a plate of the base alloy was cast under identical conditions and characterized for comparison with the composite properties.

All materials were tested in the solution-treated and naturally aged condition (T4) recommended for the Al–10Mg-matrix alloy. This heat treatment consists of an 18 h soaking at 435 °C, followed by water quenching. All test specimens were cut directly from the as-infiltrated and heat-treated billets. No working or forming of the materials was done.

Representative microstructures of composites with relatively low (25 vol %) and high (52 vol %) reinforcement contents are shown in Figs 3 and 4, respectively. The micrographs show several features of the composites. First, the large particle-size distribution of the reinforcement is clearly evident. Secondly, the low-magnification micrographs demonstrate that the composites are homogeneous, possessing no detectable gradient in filler loading. Finally, no particle–particle contacts are observed – a result of the excellent wetting.

3. Test methods

The elastic properties, tensile properties, compressive properties, and fracture characteristics were determined. The Young's modulus was measured using the resonance technique [7]. These values were subsequently confirmed by comparison to the stress–strain results obtained in both tension and compression. Good agreement was observed (within 5%); however, only the results obtained by resonant frequency are reported as they were more consistent and are assumed to be more accurate. Techniques that induce small strains, such as the resonant method, typically result in more accurate measurements. This is particularly the case with discontinuously reinforced metals where residual stresses lead to a low elastic limit, making the measurement of Young's modulus from stress–strain curves difficult [8].

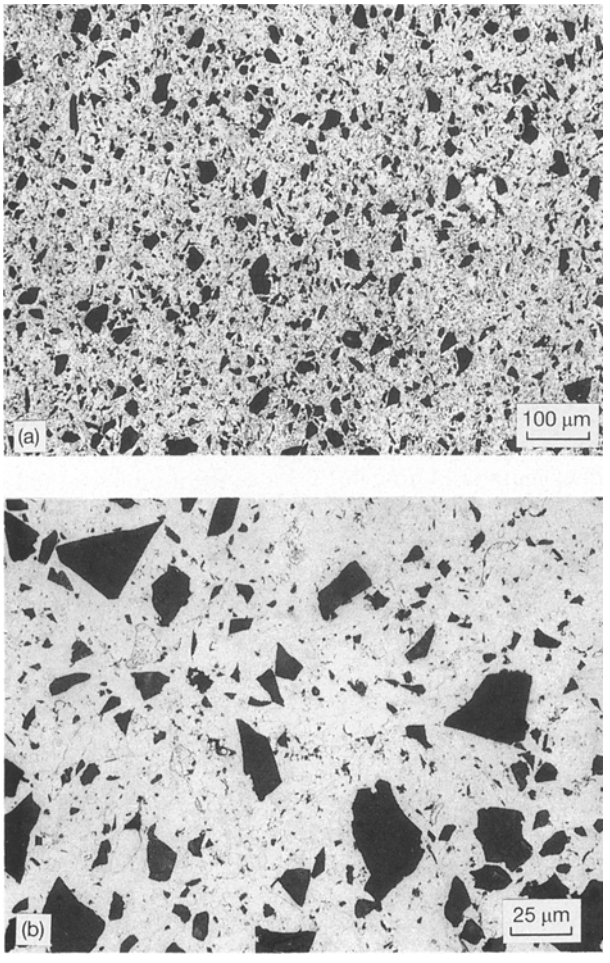

Figure 3 Optical micrographs showing a representative microstructure of an Al_2O_3/Al composite with 25 vol % reinforcement at (a) low and (b) high magnifications.

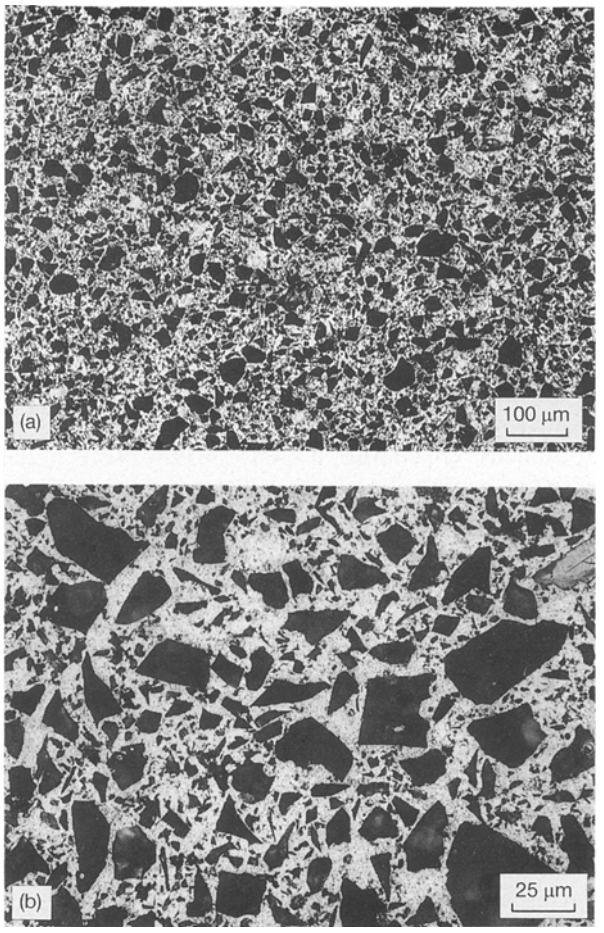

Figure 4 Optical micrographs showing a representative microstructure of an Al_2O_3/Al composite with 52 vol % reinforcement at (a) low and (b) high magnifications.

The measurements of tensile-strength properties were made using flat, reduced-gauge-section specimens in accordance with standard ASTM B557M, except that larger radii (75 mm) were employed to reduce stress concentrations. The specimens were tested at room temperature with a screw-driven, Sintech model CITS-2000, universal testing machine under displacement control at a crosshead speed of 1 mm min^{-1}. Each of the composite specimens was instrumented with a strain gauge (with a functional range of 0 to 2.5% strain) providing the strain input to the stress–strain curve. The strain in the base-metal samples, which far exceeded the range of the gauges, was measured with a laser deflectometer (Zygo model 121). The tests provided measures of tensile yield strength (0.2% offset), ultimate tensile strength, and strain-to-failure.

Compressive properties were measured according to standard ASTM E9 using cylindrical specimens

and a Tinius Olsen model 400,000-L hydraulic universal testing machine. The test specimens, which were cut and ground from billets into right circular cylinders measuring 12.5 mm in diameter by 25 mm in length, were loaded to failure between polished WC platens at 0.25 mm min^{-1} without lubrication. At small strains (less than 2.5%) the stress–strain behaviour was recorded with strain gauges bonded to the specimens, and at high strains the data was inferred from total crosshead motion as detected with a linear variable differential transformer (LVDT).

The fracture toughness was measured using a four-point-bend-chevron-notch technique and the previously mentioned Sintech universal testing machine. Specimens measuring $6 \times 4.8 \times 50$ mm were tested with the loading direction parallel to the 6 mm dimension and with inner and outer loading spans of 20 and 40 mm, respectively. The chevron notch, which was cut with a 0.3 mm wide, diamond blade, had an included angle of 60° and was located at the midlength of each specimen. The dimensions of the sample were chosen to minimize analytical differences between two calculation methods according to the analyses of Munz *et al.* [9]. Both the fracture toughness, K_q, and the critical strain-energy release rate, G_q, calculated as:

$$G_q = K_q^2(1 - \nu^2)/E \quad (1)$$

where ν is Poisson's ratio, are reported.

The chevron-notch technique is not commonly used for metal-based materials. Brown [10] measured the fracture toughness of various Al alloys by a chevron-notch technique (chevron-notched, short-bar specimens) and compared the results to accepted mode-I-plane-strain-fracture-toughness values. When the toughness of the alloy was less than 35 MPa $m^{1/2}$, good agreement between the two techniques was obtained. The present samples all fall within this range.

4. Results and discussion

Fig. 5 plots the results of Young's modulus versus the volume percentage of Al_2O_3. In addition, the Hashin–Shtrikman bounds and their average are plotted. The Hashin–Shtrikman bounds have been given by Willis [11] in the form:

$$\tilde{\kappa} = \left\{\sum_i \frac{c_i}{3\kappa_i + 4\mu}\right\}^{-1} \sum_j \frac{c_j\kappa_j}{3\kappa_j + 4\mu} \quad (2)$$

and

$$\tilde{\mu} = \left\{\sum_i \frac{c_i}{6\mu_i(\kappa + 2\mu) + \mu(9\kappa + 8\mu)}\right\}^{-1} \times \sum_j \frac{c_j\mu_j}{6\mu_j(\kappa + 2\mu) + \mu(9\kappa + 8\mu)} \quad (3)$$

where c_i is the volume fraction of the ith phase, and κ_i and μ_i are the bulk and shear moduli, respectively, of the ith phase. When κ and μ are chosen such that:

$$\kappa = \max\{\kappa_i\}, \quad \mu = \max\{\mu_i\} \quad (4)$$

the estimates $\tilde{\kappa}$ and $\tilde{\mu}$ are upper bounds, whereas choosing:

$$\kappa = \min\{\kappa_i\}, \quad \mu = \min\{\mu_i\} \quad (5)$$

results in $\tilde{\kappa}$ and $\tilde{\mu}$ being lower bounds. Bounds on Young's modulus, $\tilde{E}$, can be found from the relation:

$$\tilde{E} = 9\tilde{\kappa}\tilde{\mu}/(3\tilde{\kappa} + \tilde{\mu}) \quad (6)$$

The elastic properties of the matrix and reinforcement were used as input to Equations 2 and 3. The Al–10Mg-matrix alloy has a Young's modulus of 65 GPa and a Poisson's ratio of 0.3. The elastic properties of the reinforcement phase were estimated from the elastic properties of fully dense Al_2O_3 and the pore content of the filler particles (5 vol % average porosity). Wang [12] developed an expression for Young's modulus, E, of a porous material over a wide range of porosity (0 to 38 vol %). It is given by:

$$E = E_0\exp[-(bp + cp^2)] \quad (7)$$

where b and c are material constants that increase as the microstructure becomes more irregular; p is the volume fraction of porosity, and E_0 is Young's modulus of the material when dense. In a subsequent publication, Wang [13] investigated porous sintered Al_2O_3, which is a good approximation of the present filler material. Using 401 GPa as the modulus of fully dense Al_2O_3, the material constants b and c were found to be 1.46 and 9.82, respectively. Based on the average level of porosity in the filler, Young's modulus can be estimated as 363 GPa.

The Hashin–Shtrikman bounds are known to be optimal for the case of a binary composite. Where the properties of a given composite lie with respect to these bounds depends on the structure of the composite. For instance, consider two concentric spheres with material A on the outside and material B on the inside, with the ratio of the radii chosen to provide the desired volume fraction of B in A. A binary composite can be constructed by assembling many of these spheres, of different sizes, so that the composite will be homogeneous and isotropic on a scale that is large compared with the size of the spheres, and the volume fraction of B in A will be the same as that of the individual spheres. If material A is more compliant

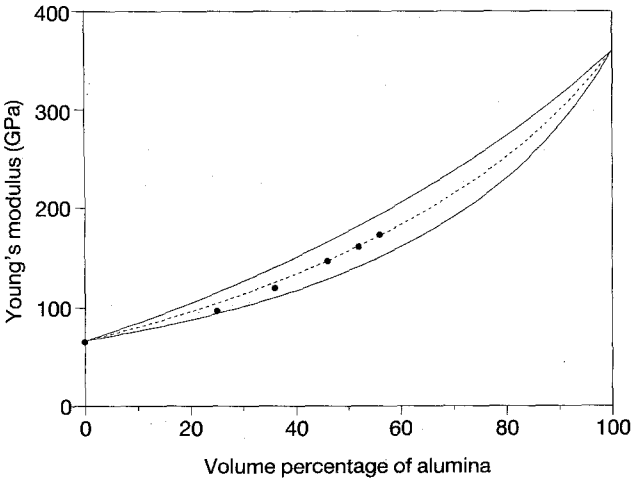

Figure 5 Young's modulus of Al_2O_3/Al composites as a function of Al_2O_3 content. (●) The measured values, (—) the Hashin–Shtrikman predictive bounds and (– – –) the average of the upper and lower bounds.

than material B, the composite's elastic moduli will lie on the Hashin–Shtrikman lower bound, whereas if material A is stiffer than material B, the composite's elastic moduli will lie on the upper bound [14].

In the present metal-matrix composites, the continuous phase is more compliant. As the volume fraction of Al_2O_3 decreases, there is more matrix metal separating the filler particles. Thus, as the volume fraction of reinforcement falls, the composite properties should begin to fall closer to the lower bound than to the upper bound. As is shown in Fig. 5, the data does follow this trend. Rohatgi *et al.* [15] have also observed that the measured Young's moduli of discontinuously reinforced metal-matrix composites more closely follow the lower bound at low reinforcement levels.

The tensile strength results are shown in Figs 6 and 7. Fig. 6 plots the measured values of 0.2% offset yield strength and ultimate tensile strength versus the volume percentage of Al_2O_3. Each data point on the curve is an average from at least six independent tensile tests. Both curves show an increase in strength with increasing Al_2O_3 content, with a greater rate of increase in the more highly loaded region of the curves. Moreover, as the loading increases, which results in a lower ductility, the difference between the yield and ultimate strength is reduced.

Fig. 7 plots individual stress–strain curves for each material. The difference in elastic modulus and strength between the materials is clearly demonstrated. In addition, the effect of particulate loading on ductility is shown. The composites show a gradual drop in strain-to-failure with increasing Al_2O_3 content, whereas the base alloy possesses a strain-to-failure which is approximately an order of magnitude greater than that of the composites. Again, the limited ductility of the more highly loaded composites leads to similar values of yield and ultimate strength to those shown in Fig. 6.

The results of compressive yield (0.2% offset) and ultimate strength versus particulate loading are shown in Fig. 8a and b, respectively. Each data point on the curves is an average value from at least four independent tests. As with the tensile yield strength, the compressive yield strength increases at an increasing rate with loading.

There is little difference between the tensile and compressive yield strengths, which can be seen by comparing Figs 6 and 8a. Additionally, Fig. 9, which plots both the tensile and compressive stress–strain

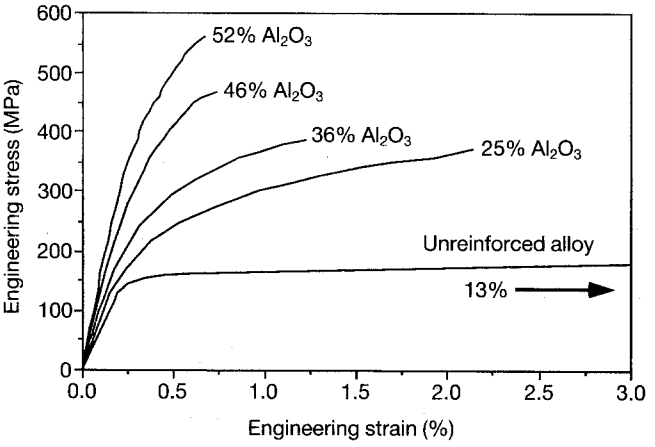

Figure 7 Individual tensile stress–strain curves for Al_2O_3/Al-composite specimens with different reinforcement contents.

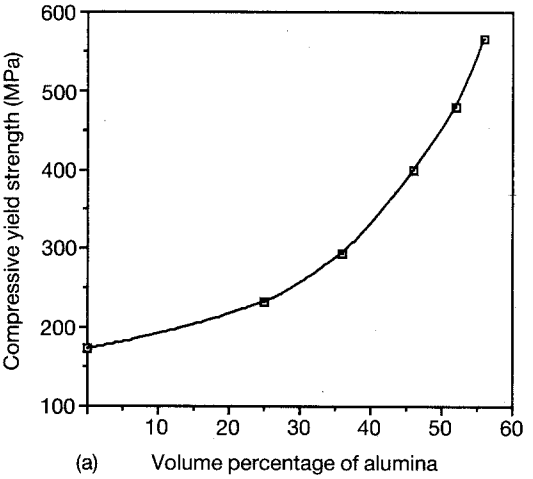

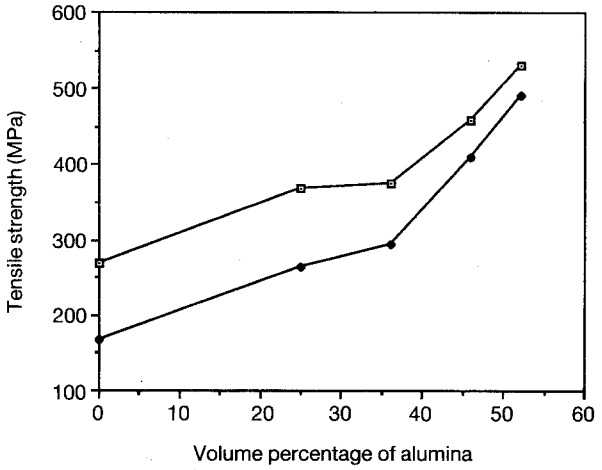

Figure 6 (◆) Tensile yield strength (0.2% offset) and (⊡) ultimate tensile strength of Al_2O_3/Al composites as a function of Al_2O_3 content.

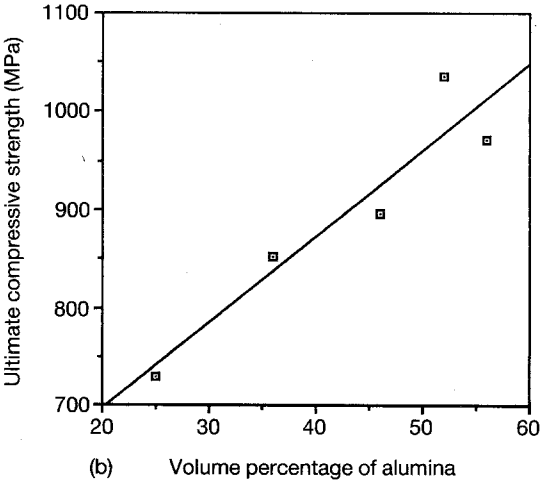

Figure 8 (a) Compressive yield strength (0.2% offset) and (b) ultimate compressive strength of Al_2O_3/Al composites as a function of Al_2O_3 content.

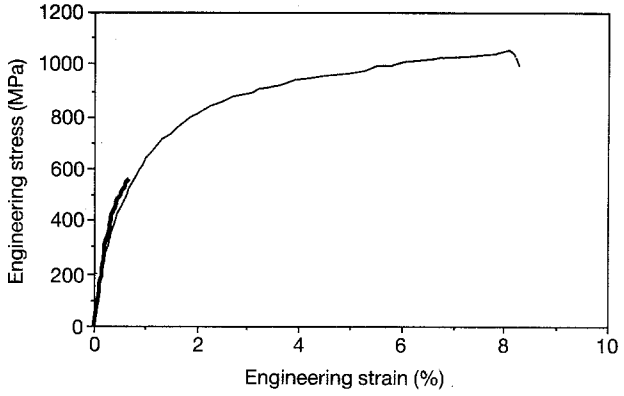

Figure 9 Comparison of (–) tensile and (—) compressive stress–strain curves for Al_2O_3/Al composite containing 52 vol % reinforcement. The two curves display similar initial slopes (moduli) and yield points, but the compression sample ultimately failed at much higher stresses and strains.

curves for the 52 vol % Al_2O_3 sample, shows the two curves to be similar up to the point of tensile failure. This follows the work of Arsenault and Wu [16], who predicted and observed little difference in tensile and compressive yield strength when equiaxed particulate reinforcement was employed.

The difference between the ultimate tensile and compressive strengths, however, is significant. For instance, the tensile curve in Fig. 9 shows failure at less than 1% strain, whereas the compression curve extends to a strain of more than 8%. The compression sample failed at an ultimate strength nearly double that of the tensile specimen (over 1000 MPa). Note that a value of ultimate compressive strength for the base alloy was not obtained as only plastic deformation (i.e. no fracture) was obtained.

Fig. 10 plots the fracture-toughness results. Both the measured value of K_q and the calculated value of G_q, from Equation 1, are provided. Again, each data point is an average value from a minimum of six specimens. For the composites, K_q is unaffected by loading, with a value near 20 MPa $m^{1/2}$, whereas G_q decreases as the Al_2O_3 content increases due to the change in Young's modulus. This result of more-or-less-constant critical-stress intensity (toughness) but decreasing strain-energy release rate (fracture energy) with increasing loading has been previously observed [17]. The value of K_q for the base alloy is about 50% higher than that of the toughest composite.

Fig. 11 shows low-magnification SEM micrographs of tensile fracture surfaces of the composites containing 25 and 52 vol % Al_2O_3. The same failure process is seen in both composites. The ceramic fails via transgranular fracture, with the fracture occurring through the particulates on the same plane as the propagating crack. No pull-out of the particulates is observed. The Al-alloy matrix fails in a ductile manner by a void-nucleation and growth mechanism with the diameter of the voids reaching no more than 10 μm.

The nature of the interface between the ductile matrix and the brittle reinforcement is shown in Fig. 12 with a high-magnification SEM micrograph of a tensile fracture surface of the composite containing 25 vol % Al_2O_3. There is an excellent bond between

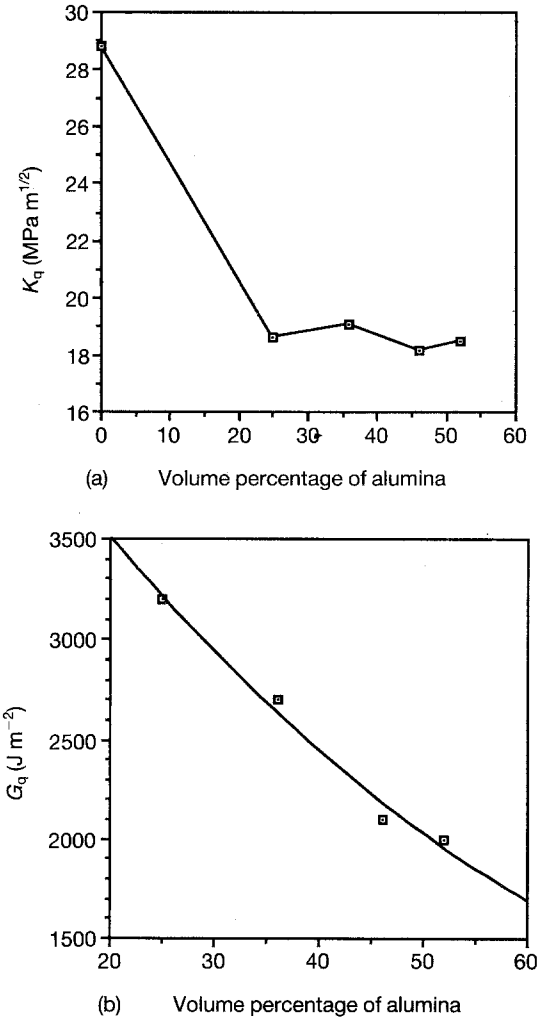

Figure 10 (a) Fracture toughness, K_q, and (b) critical-strain energy-release rate, G_q, of Al_2O_3/Al composites as a function of Al_2O_3 content.

the two phases, with no separation evident. This strong bond allows for good load transfer between the two phases. To obtain maximum strengthening, load transfer via a strong matrix to reinforcement bond is necessary [18]. Thus, as the content of the strong and stiff reinforcement increases, the strength of the composite increases (Figs 6 and 8). However, the load transfer cannot account for the non-linear increase in strength with increasing loading.

A second result of the bond between the reinforcement and matrix phases is an imposed constraint on the metal phase. That is, when an external load is applied, the Al-alloy matrix is constrained from lateral motion since it is bonded to the stiff-reinforcement particles. When laterally constrained (i.e. when the material is under a triaxial stress state), the apparent yield strength of a metal is increased. The relationship between the normal yield strength, σ_y, and the apparent yield strength under lateral constraint, σ_{ycon}, is given by:

$$\sigma_{ycon} = \sigma_y(1 - \nu)/(1 - 2\nu) \quad (8)$$

where ν is Poisson's ratio. This relationship derives from the loading conditions for one-dimensional strain, the generalized Hooke's law, and the Von Mises' yield criterion for isotropic materials, and

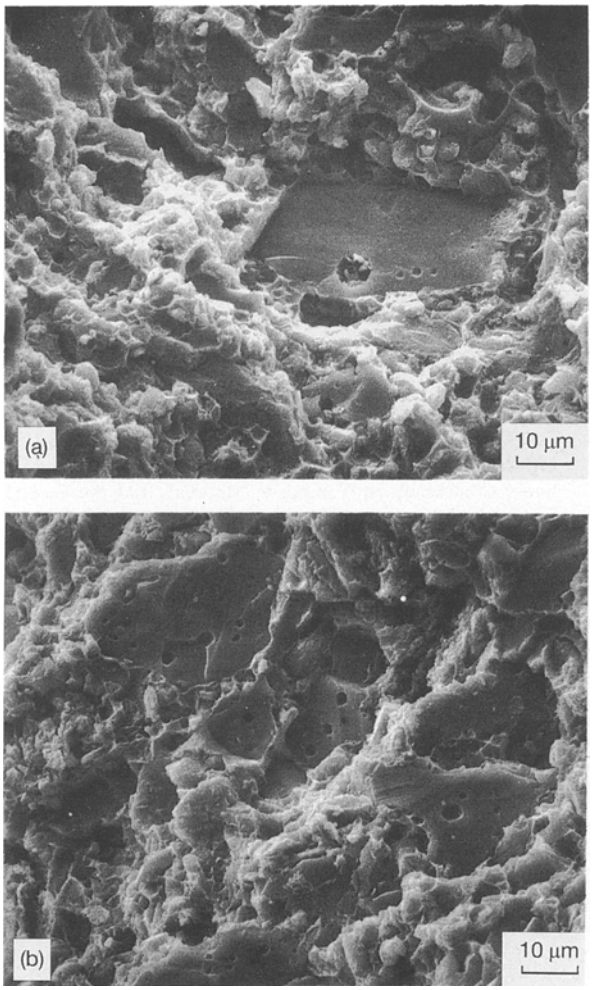

Figure 11 Low-magnification SEM micrographs of tensile fracture surfaces of Al_2O_3/Al composites containing (a) 25 and (b) 52 vol % reinforcement.

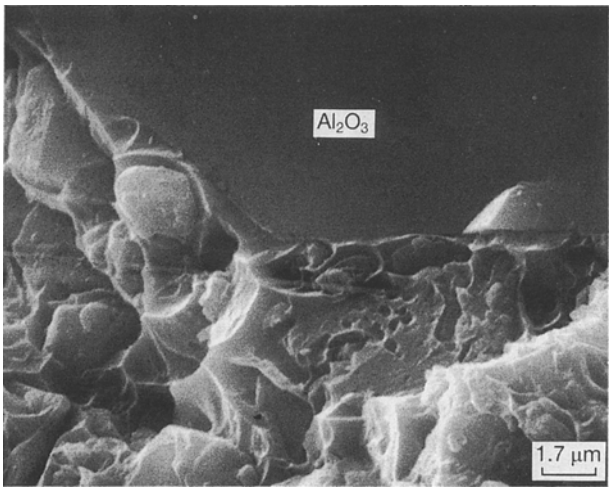

Figure 12 High-magnification SEM micrograph of Al_2O_3/Al composite containing 25 vol % reinforcement. An excellent bond between the two phases is observed.

predicts a two-times increase in yield strength for a metal with a Poisson's ratio of 0.33. Working with 2024 Al in various heat-treatment conditions, Rosenberg *et al.* [19] found this relationship to be obeyed over a wide range in yield strength.

In a particulate-reinforced composite, the matrix is never fully constrained. For a well-bonded, high-modulus particle, constraint of the matrix should be at a maximum near the reinforcement and should fall off with distance from the interface to the midpoint between particles. Therefore, the greater the interfacial surface area and the smaller the distance between particles, the greater the mean matrix constraint. For a given particle-size distribution, the ratio of the interfacial area to the volume of the matrix is proportional to $V_p/(1 - V_p)$, where V_p is the volume fraction of particles. The inverse of the spacing between interfaces would be dependent on the particle geometry, but for cubic particles in a cubic array, it would be proportional to $V_p^{1/3}/(1 - V_p^{1/3})$. Since both of these functions increase without limit as V_p approaches 1, the yield strength of the matrix (i.e. the mean matrix constraint) would be expected to increase with particle loading and to accelerate as the loading increased, as has been experimentally observed.

5. Conclusions

Particulate-reinforced Al_2O_3/Al metal-matrix composites with various particulate loadings were fabricated by a pressureless-liquid-metal-infiltration process. The elastic, tensile, compressive and fracture properties were evaluated, and the results were related to the reinforcement content. The following conclusions were obtained.

1. Increases in reinforcement content resulted in systematic increases in Young's modulus, with the highest loaded composite that was investigated (56 vol %) having a stiffness of over 2.5 times that of the base alloy. At high loadings (46 vol % and above) the average of the Hashin–Shtrikman bounds provided an excellent prediction of Young's modulus, whereas at lower loadings (36 vol % and below) the data fell closer to the lower bound than to the upper bound.

2. The tensile yield (0.2% offset) and ultimate strengths increased with reinforcement content, and the rate of increase in strength was highest in the more highly loaded composites. The strongest composite possessed tensile yield and ultimate strengths 2.8 and 2 times greater, respectively, than those of the unreinforced base alloy.

3. To the yield point (0.2% offset), the composites behaved nominally the same under both tensile and compressive loads; however, the compressive samples were able to accommodate far more strain before failing and achieved very high ultimate strengths. The strongest composite had an ultimate compressive strength of greater than 1 GPa.

4. The fracture toughnesses, K_q of the composites were near 20 MPa $m^{1/2}$, regardless of loading, compared to a value of about 29 MPa $m^{1/2}$ for the base alloy. The critical-strain-energy release rate, G_q increased as loading decreased due to a simultaneous reduction in Young's modulus.

5. With fractography, the failure of the composites was shown to consist of transgranular fracture of the Al_2O_3 reinforcement and ductile rupture of the Al-alloy matrix.

6. The strong matrix-to-reinforcement bond, qualitatively shown with fractography, leads to a partial lateral constraint of the metallic phase upon loading. This constraint, which increases with reinforcement content, is a possible explanation for the non-linear increase in strength with particulate loading.

Acknowledgement

Helpful discussions with Prof. Pedro Ponte-Casteñada of the Department of Mechanical Engineering at the University of Pennsylvania are gratefully acknowledged.

References

1. D. L. McDANELS, *Metall. Trans. A* **16** (1985) 1105.
2. J. M. PAPAZIAN and P. N. ALDER, *ibid. A* **21** (1990) 401.
3. J. W. McCOY, C. JONES and F. E. WARNER, *SAMPE Q.* **19**(2) (1988) 37.
4. P. K. GHOSH and S. RAY, *J. Mater. Sci.* **21** (1986) 1167.
5. M. K. AGHAJANIAN, J. T. BURKE, D. R. WHITE and A. S. NAGELBERG, *SAMPE Q.* **20**(4) (1989) 43.
6. M. K. AGHAJANIAN, M. A. ROCAZELLA, J. T. BURKE and S. D. KECK, *J. Mater. Sci.* **26** (1991) 447.
7. S. SPINNER and W. E. TEFFT, *ASME Proc.* **61** (1961) 1221.
8. T. G. NIEH and D. J. CHELLMAN, *Scripta Metall.* **18** (1984) 925.
9. D. G. MUNZ, J. L. SHANNON and R. T. BUBSEY, *Int. J. Fracture* **16** (1980) R137.
10. K. R. BROWN, in "Chevron-notched specimens: testing and stress analysis, ASTM STP 855", edited by J. H. Underwood, S. W. Freiman and F. I. Baratta (American Society for Testing and Materials, Philadelphia, 1984) pp. 237–54.
11. J. R. WILLIS, in "Mechanics of solids, Rodney Hill 60th anniversary Vol.", edited by H. G. Hopkins and M. J. Sewell (Pergamon Press, Oxford, 1982) pp. 653–86.
12. J. C. WANG, *J. Mater. Sci.* **19** (1984) 801.
13. *Idem. ibid.* **19** (1984) 809.
14. Z. HASHIN and S. SHTRIKMAN, *J. Mech. Phys. Solids* **11** (1963) 127.
15. P. K. ROHATGI, S. RAMAN, B. S. MAJUMDAR and A. BANERJEE, *Mater. Sci. Engng. A* **123** (1990) 89.
16. R. J. ARSENAULT and S. B. WU, *ibid.* **96** (1987) 77.
17. F. GIROT, J. M. QUENISSET, R. NASLAIN, B. COUTLAND and T. MACKE, in Proceedings of the Sixth International Conference on Composite Materials and the Second European Conference on Composite Materials, London, UK, Vol. 2, edited by F. L. Matthews, N. C. R. Buske, J. M. Hodgkinson, and J. Morton (Elsevier Applied Science, London, 1987) pp. 330–9.
18. B. ROEBUCK, *J. Mater. Sci. Lett.* **6** (1987) 1138.
19. Z. ROSENBERG, Y. PARTOM and Y. YESHURUN, *J. Phys. D* **15** (1982) 1137.

Received 9 November 1992
and accepted 21 April 1993